HIROSAKI UNIVERSITY

REM
Radiat Environ Med

Radiation Environment and Medicine 2021 Vol.10, No.1 37–47

Regular Article

Study of Meteorological Influence on the Count of ^{222}Rn and ^{220}Rn Gases and Its Possibility for a Forecasting Gas

T Thuamthansanga[1], Bijay Kumar Sahoo[3], Ramesh Chandra Tiwari[1]* and Raghavendra Prasad Tiwari[2]

[1]*Department of Physics, Mizoram University, Aizawl-796004, Mizoram, India*
[2]*Department of Geology, Mizoram University, Aizawl-796004, Mizoram, India*
[3]*Radiological Physics and Advisory Division, Bhabha Atomic Research Centre, Mumbai, 400085 Maharashtra, India*

Received 9 July 2020; revised 8 November 2020; accepted 18 November 2020

The study investigates the influence of meteorological factors on the count of ^{222}Rn and ^{220}Rn gases at the interest of observing them as a possible forecasting gas to geophysical phenomena. The study was carried out between May, 2018 and October, 2018 at the soil-air interface using a ZnS (Ag) scintillator counter (Model: *SMARTRnDuo*, BARC, India). Data's were generated *in-situ* online and was the first of its kind for the region. The backward multiple linear regression analysis shows that pressure was the most effecting variable on radon data, while no significant correlation was observed between thoron and meteorological data. The observed weak correlation between the isotope pair data and most of the meteorological factors reveals activeness of action taken against the factors, while acquiring data. Concentrations and fluxes of the isotope pair, content of ^{238}U and ^{232}Th and their comparison with the worldwide average were also presented. It is also observed that radon data of the continuous monitoring station (CMS) and Mat fault varies in proportion during geophysical process, while no geophysical properties of ^{220}Rn were observed. The study reveals the reason behind radon anomaly was geophysical activity but not meteorological factors.

Key words: Radon, meteorological parameters, geophysical phenomena, anomalous, correlation

1. Introduction

Radon is a radioactive noble gas having three naturally occurring isotopes viz. radon (^{222}Rn, $T_{1/2}$=3.825 days), thoron (^{220}Rn, $T_{1/2}$=55.6 s) and actinon (^{219}Rn, $T_{1/2}$=3.6 s). Actinon has been neglected in this study due to its extremely small half-life. ^{222}Rn and ^{220}Rn have a typical diffusion length of 1 m and 1 cm in the soil, respectively[1].

*R.C. Tiwari: Department of Physics, Mizoram University, Aizawl-796004, Mizoram, India
E-mail: ramesh_mzu@rediffmail.com

Copyright © 2021 by Hirosaki University. All rights reserved.

The general diffusion equation for radon in a typical soil is given by equation (1)[1, 2]

$$\frac{\partial C_p}{\partial t} = S - \nabla \cdot F_p - \lambda C_p \quad (1)$$

Where S is the radon activity released into a unit volume of the pore space per unit time, F_p is the activity of radon crossing per unit pore area per unit time and C_p is the radon activity per unit pore space volume (radon concentration in pore space).

Being originated in the earth crust, radon has been

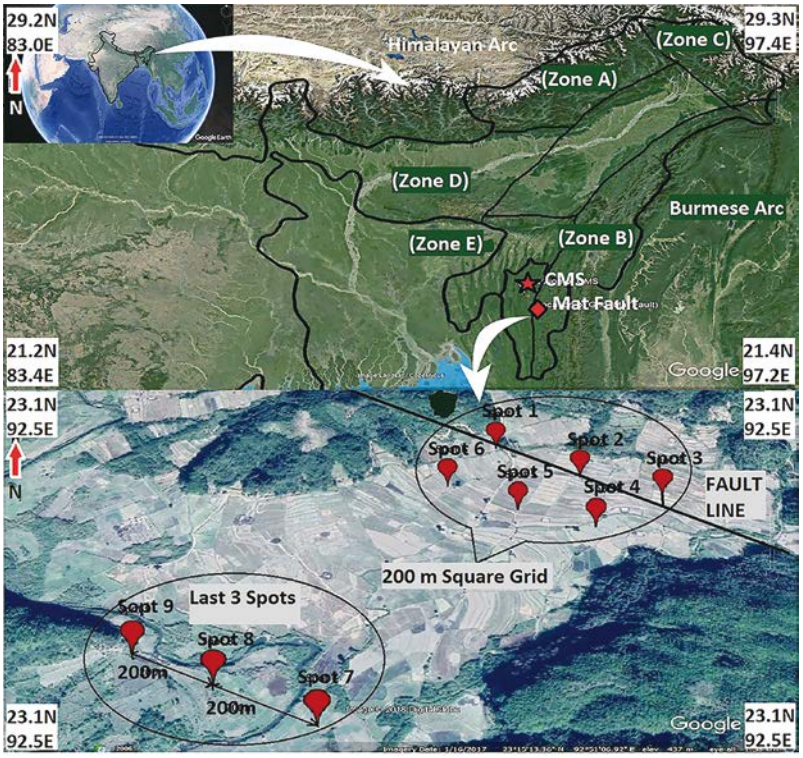

Fig. 1. Map of India and Northeast India, showing locations of the continuous monitoring station (CMS) and formation of rectangular grid at Mat Fault located at 57 km from the CMS.

measured as a tracer to fault system, uranium and thorium deposit and for estimating its radiological risks input to the atmosphere[2, 3]. A renaissance in radon monitoring occurs after observation of its anomaly before the Tashkent earthquake in 1966[4]. The observation ignites optimistic motivation to many researchers and was instantly followed up by researchers from China, Japan and USA in the year 1973, 1975 and 1978, respectively[4, 5]. With successive positive result in soil and ground water, shortly measurement of radon as a premonitory gas to earthquakes became a worldwide pheomena[6-17]. Radon anomaly due to seismic activity was not only observed in the soil and water but also in the atmosphere, hydrothermal system and mud-volcano[18-24]. Despite the tireless effort, radon monitoring for earthquake prediction was still with uncertainties and needs improvement in many ways. Among them was minimization of the meteorological influence, which must be identified and removed to avoid false prediction. In the present study it has been achieved by insulating the continuous monitoring station (CMS) from all sides at Mizoram University. The study area in particular northeast India was declared as one of the highest seismic zone (Zone V) by seismic hazard zonation map of India[25]. But it has a very limited and immature literature[16, 26-33] on premonitory studies of geophysical phenomena base on radon data. Besides, the data were passive[16, 26-31] in nature with large sampling interval and lack the real time nature of radon variation. To improve the measurement and for better understanding of the real time characteristics, 15 minutes cycle radon data were generated between May, 2018 and October, 2018 at Mizoram university. At the same time *in-situ* data of radon was generated at mat fault for comparative analysis (Fig. 1). The outline of the study may be listed as follows:

(i) Generating 15 minutes and 1 month frequency radon isotope pair (^{222}Rn and ^{220}Rn) data at Mizoram University and Mat fault, respectively for six month.
(ii) Correlating the isotope pair data with meteorological data in order to observe meteorological influence on counts of the isotope pair.
(iii) Obtaining ^{222}Rn and ^{220}Rn flux and estimating ^{238}U and ^{232}Th content of the region from their respective daughter nuclei.
(iv) Observing the possibility of radon as a forecasting gas to geophysical phenomena by comparing data of the two locations.

The ^{222}Rn and ^{220}Rn data were collected using an indigenously developed and calibrated ZnS(Ag) scintillator counter (Model: *SMARTRnDuo*, BARC, India). The meteorological data on the other hand were obtained from the nearest meteorological station, IMD-Regional Meteorological Centre, Guwahati, Assam (India). A backward multiple linear regression (MLR)

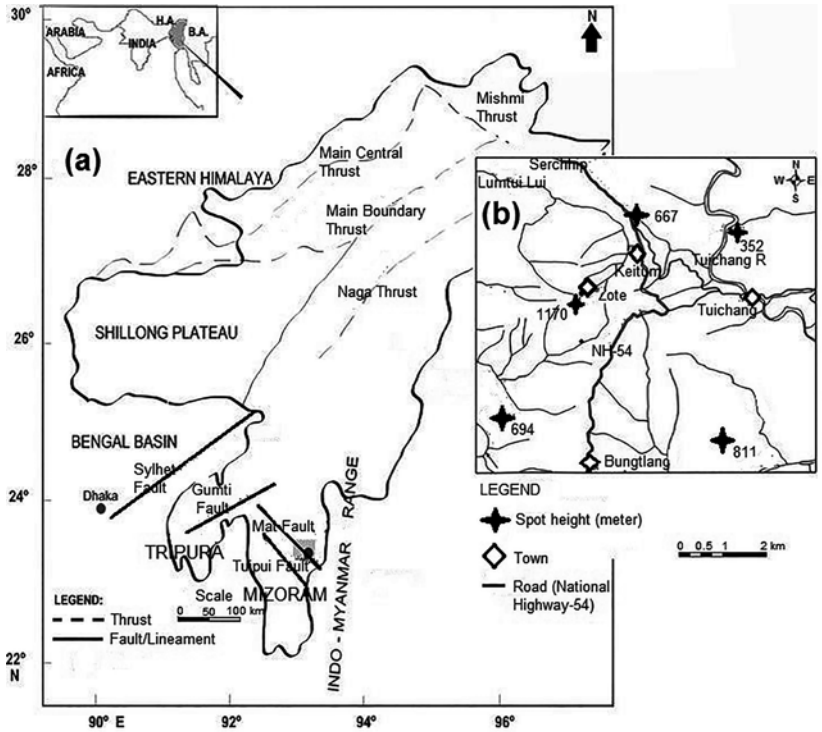

Fig. 2. (a) Geological map of northeast India showing major lineaments/faults in Tripura-Mizoram fold belt (modified after Jaishi and group[27]), (b) Geological map of the of the study region.

analysis was performed to observe the extent of meteorological influence on the isotope pair data and the most influencing factors. Possible response of radon count to geophysical phenomena, ^{238}U and ^{232}Th content of the region and their comparison to the global average and critical value given by UNSCEAR[34] and IAEA[35], respectively were presented in details.

2. Geological Setup of the Region

Northeast India and specifically Mizoram was situated at the junction of Himalayan Arc to the north and Burmese Arc to the east (Fig. 1 & 2). The northeast region based on distribution of its epicentres, fault plane solutions and geotectonic features was divided into five seismotectonic zones[28, 29, 36]. They are as follows, (i) Eastern Himalayan collision zone (zone A) (ii) Indo-Myanmar subduction zone (zone B), (iii) Syntaxis zone of Himalayan arc and Burmese arc (Mishmi Hills, zone C) (iv) Plate boundary zone of the Shillong plateau and Assam valley (zone D) and (v) Bengal basin and plate boundary zone of Trpura-Mizoram fold belt (zone E) (Fig. 1). The collision tectonic between Eurasian plate and Indian plate at the north and subduction tectonics at the east attributes seismicity of the region and is one of the most dynamic sectors of the present day crust[37]. The provinces were extended to the adjoining territories like Tibet, Baladesh, Myanmar and some even extended beyond the shorelines into the Bay of Bengal. In addition Mizoram belongs to the Surma basin which is part of the greater Bengal Basin. The basin is an area of folded sediment which is wider to the north and narrower to the south with many NE-SW and NW-SE trending lineaments/faults (Fig. 2). The NE-SW Syllhet fault running from near Dhaka (Bangladesh) demarcates the northwestern boundary of the Surma basin while the Gumti fault cut across the basin. Among the NW-SE trending faults, Mat fault and Tuipui fault lies within Mizoram at the southern part of the basin (Fig. 2). Mat fault is one of the most prominent faults in Mizoram which obliquely cut across the Indo-Burmese Arc (NS-trend) and is traceable across the entire state from satellite and Google maps[26, 27]. According to seismic hazard zonation map of India, northeast India lies at zone V, the highest seismic activity and is one of the six most seismically active region of the world along with Taiwan, Japan, Mexico, California and Turkey[38]. In the present study Mat fault being the most prominent faults within the state was selected for generating *in-situ* data.

3. Materials and Methods

3.1. Continuous radon monitor-SMARTRnDuo

SMARTRnDuo is a ZnS(Ag) scintillator based counter developed and calibrated by Bhabha Atomic Research

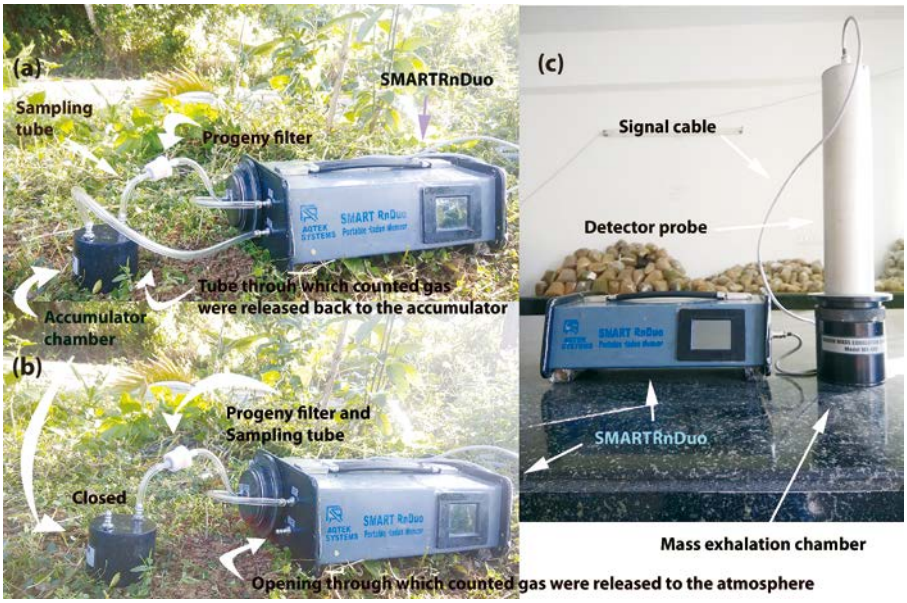

Fig. 3. Schematic diagram of the experimental setup of SMARTRnDuo for (a) Measurement at the CMS using accumulator chamber of 3.1×10^{-5} m^3 (b) Measurement at the rectangular grid (Mat fault) using accumulator chamber of 2.1×10^{-4} m^3 (c) Measurement of mass exhalation rate of soil sample.

Centre, Mumbai, India. It has a dimension of 37 cm×20 cm×12 cm and equipped with a scintillation cell of volume 153 cm^3, an internal battery of 6 V, electronic system for recording, displaying and transferring data to a PC. The scintillation cell is internally coated with ZnS (Ag) scintillator and has a measurement range of 8 Bq m^{-3} -50 MBq m^{-3} and 15-50 MBq m^{-3} for ^{222}Rn and ^{220}Rn, respectively at 63% confidence level (1σ) for 1-hour cycle. The cell has a sensitivity of 1.2 counts per hour (cph)/(Bq m^{-3}) and 0.8 cph/(Bq m^{-3}) for ^{222}Rn and ^{220}Rn, respectively. The sampling flow rate into the instrument was 0.5-0.7 L/min (maintained by an inbuilt pump) and attains 95% of ^{222}Rn/^{220}Rn concentration in a response time of 15 minutes. The instrument is operable in three modes, radon mode, thoron mode and alpha mode with a selectable cycle of 15, 30 and 60 minutes for each of the mode. In the present study, the monitor was operated in thoron mode with 15 minutes cycle at the monitoring station as well as in the fault. In thoron mode, both alpha particles from ^{222}Rn and ^{220}Rn gases were counted for retrieving their concentrations[32, 33, 39-41].

3.2. Technique for measurement using SMARTRnDuo

A continuous monitoring station (CMS) for ^{222}Rn and ^{220}Rn gases was set up at the Department of Physics, Mizoram University, Aizawl, Mizoram (India). It is a 4 m^2 area station (taking care of the 1 m and 1 cm diffusion length of ^{222}Rn and ^{220}Rn gases from all sides when placed the accumulator chamber at the centre). Since it has been covered with insulating sheets from all sides, the effect of meteorological factors on the exhalation of the isotope pair was believed to reduce to great extend compare to that of an open space. Considering the advantage of rapid equilibrium in a small chamber in comparison to a large chamber, an accumulator having a volume of 3.1×10^{-5} m^3 was used at the centre of the CMS and connected to the SMARTRnDuo using a rubber tube forming a closed-loop system (Fig. 3a). The monitor was operated with 15 minutes cycle continuously for 24 hours where the accumulated gases get circled after every 15 minutes. In this manner, any abnormal addition or reduction in concentrations of the gases within the exhalation chamber can be easily noticed. During the first 5 minutes of the 15 minutes cycle, simultaneous sampling and counting of radon and thoron data was performed. The next 5 minutes was delayed to cut off the short-lived thoron (55.6 s), hence alpha counts of the last 5 minutes attributes to that of radon concentration. Then the thoron counts were obtained by subtracting the last 5 minutes counts from the first 5 minutes counts[2].

At Mat fault, the ^{222}Rn and ^{220}Rn data were generated from a rectangular grid (1000 m×400 m) of 9 spots (Fig. 1). The first six spots formed a square grid where three of them lies within the fault line and the other three at a distance of 200 m from the fault line adjacent to the first three spots within the fault. The last three spots were at a distance of 1000 m from the fault line adjacent to the first six spots within and near the fault line. An accumulator chamber of volume 2.09×10^{-4} m^3 was deployed for measuring the *in-situ* flux of the isotope pair. The operating manual of the instrument was the same as that of the CMS mention above except that it was in open loop

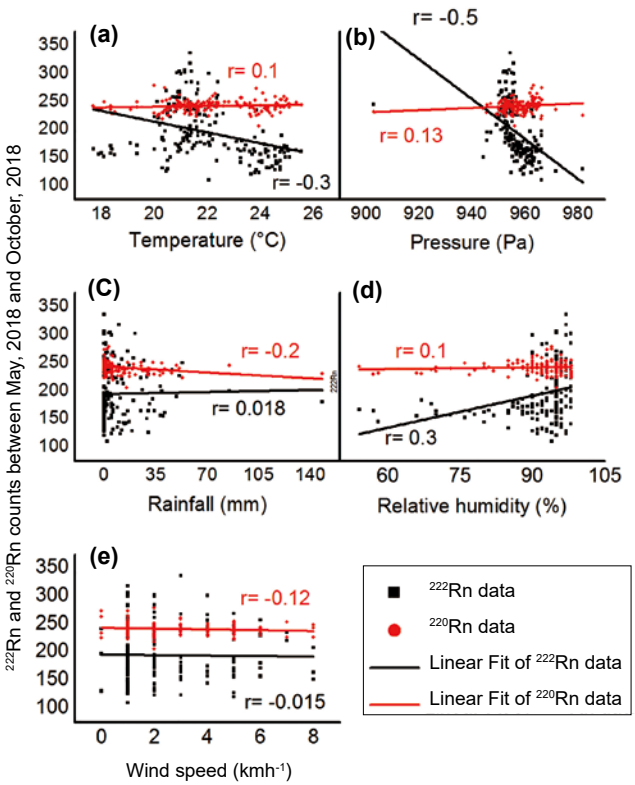

Fig. 4. Plot of ^{222}Rn and ^{220}Rn data versus (a) air temperature, (b) pressure, (c) rainfall, (d) humidity and (e) wind speed.

and the counted gases were released into the atmosphere (Fig. 3b). After completing 15 minutes cycle in Spot 1 it was proceeded to spot 2 and so on according to their serial number till spot 9. In this manner, *in-situ* online ^{222}Rn and ^{220}Rn data were generated between May, 2018 and October, 2018 at Mat fault[32, 33, 39-41].

To observe the influence of meteorological factors on ^{222}Rn and ^{220}Rn counts, the generated data's were correlated with meteorological parameters (air temperature, pressure, rainfall, humidity and wind speed) obtained from IMD-Regional Meteorological Centre, Guwahati, Assam (India). For statistical analyses (Pearson correlation and significant t-test) and result display, Microsoft Excel 2013 and Origin 8 (OriginLab Corporation) and SPSS statistical package were used.

4. Results and Discussion

4.1. Influence of meteorological factors on ^{222}Rn and ^{220}Rn Data

The meteorological effect on ^{222}Rn and ^{220}Rn data was analysed by a two-tail t-test at 95% confidence level. In the analysis, data's of Mat fault were neglected due to small sample size, such that, it takes part only in inter-comparison with the CMS data in depicting geophysical phenomena. On the other hand, data's of the CMS were used as a reference for Mat fault data and as well for correlating with meteorological data.

When correlated with meteorological data (air temperature, barometric pressure, rainfall, relative humidity and wind speed), thoron shows a negligible correlation with all the meteorological parameters (Fig. 4(a-e), Table 1). The p-value of the correlation was greater than the significance level (0.05) in all the cases except for rainfall (p = 0.0008). Hence in general, it was confirmed that no significance meteorological influence was observed on ^{220}Rn data during the study period. In other words, the extent of meteorological influence on ^{220}Rn gas of the present location was not understood except for rainfall. Radon data, on the other hand, shows zero correlation with precipitation and wind speed. It also shows a weak direct and reverse correlation with humidity and air temperature, respectively and a moderate reverse correlation with pressure (Fig. 4(a-e), Table 1). When tested the significance of the correlation, the *p*-value of precipitation and wind speed was greater than the significance level, while that of relative humidity, air temperature and pressure were lower than the significance level. Hence the counts of ^{222}Rn might be mildly affected by humidity, temperature and pressure. Now to observe the best predictor, a backward multiple linear regressions was performed through different model. In the first model the dependent variable (Radon) was regressed with all the predictor variables (air temperature, pressure, rainfall, humidity, wind speed). In the next model variables with the highest p-value was excluded to improve the model. The exclusion of the variables in the succeeded model was completely based on the p-value being the highest in the previous model regardless of whether it is significant or not. And the process was repeated until no candidate predictor was available. The raw score multiple linear regression was given by equation (2)[16, 29] and facilitates the study of several independent variables for a given independent variable.

$$Y' = a + b_1X_1 + b_2X_2 + b_3 + X_3 + \ldots\ldots + b_n + X_n \qquad (2)$$

Where Y' is the predicted value of the dependent variable, a is the constant term, b_1, b_2, ..., b_n are the regression coefficient and X_1, X_2, ..., X_n are the independent variables. But the regression coefficient of equation (2) depends on the unit of the independent variable; hence it was not appropriate to compare the independent variables amongst themselves to find out the most influencing independent variables on the dependent variables. To overcome this problem both the coefficient and variables were standardised using equation (3)[29] which facilitate direct comparison among the predictors.

Table 1. Details of correlation between ^{222}Rn and ^{220}Rn counts with meteorological parameters (air temperature, pressure, rainfall, humidity and wind speed) using two-tail t-test at significant level of 0.05

		Temperature (℃)	Humidity (%)	Rainfall (mm)	Pressure (Pa)	Wind speed (km h^{-1})	^{222}Rn count	^{220}Rn count
Temperature (℃)	r	1	0.2	-0.3	0.3	-0.5	-0.3	0.1
	Sig.		0.0009	0.0004	0.0001	7.4×10^{-12}	2.2×10^{-6}	0.2
Humidity (%)	r		1	0.04	-0.3	-0.1	0.3	0.1
	Sig.			0.6	0.0006	0.2	4.7×10^{-5}	0.3
Rainfall (mm)	r			1	-0.2	0.1	0.02	-0.2
	Sig.				0.01	0.1	0.8	0.001
Pressure (Pa)	r				1	-0.2	-0.5	0.1
	Sig.					0.002	1.1×10^{-11}	0.1
Wind speed (kmh^{-1})	r					1	-0.02	-0.1
	Sig.						0.8	0.1
^{222}Rn count	r						1	0.1
	Sig.							0.1
No. of data points		180	180	180	180	180	180	180
^{220}Rn count	r							1

Table 2. Different models of the backward multiple linear regression and its output using a two tail t-test

	Model	Unstandardized coefficients		Standardized coefficients beta	t-value	Sig. (*p*-value)
		B	Std. Error			
1	(Constant)	2900	460		6.3	2.3×10^{-9}
	Temperature (℃)	-14	2.0	-0.50	-7.1	3.7×10^{-11}
	Humidity (%)	2.0	0.40	0.31	4.9	1.8×10^{-6}
	Rainfall (mm)	-0.46	0.17	-0.16	-2.7	7.0×10^{-3}
	Pressure (Pa)	-2.7	0.47	-0.36	-5.6	8.2×10^{-8}
	Wind speed (km h^{-1})	-8.0	1.8	-0.29	-4.5	1.3×10^{-5}
2	(Constant)	2800	460		5.9	1.5×10^{-8}
	Temperature (℃)	-13	2.0	-0.46	-6.5	8.0×10^{-10}
	Humidity (%)	1.9	0.40	0.30	4.7	6.2×10^{-6}
	Pressure (Pa)	-2.5	0.48	-0.34	-5.3	3.6×10^{-7}
	Wind speed (km h^{-1})	-7.9	1.8	-0.29	-4.3	2.5×10^{-5}
3	(Constant)	2400	480		5.0	1.1×10^{-6}
	Temperature (℃)	-9.2	1.9	-0.33	-4.9	1.9×10^{-6}
	Humidity (%)	1.9	0.43	0.30	4.5	1.1×10^{-5}
	Pressure (Pa)	-2.3	0.50	-0.31	-4.6	8.3×10^{-6}
4	(Constant)	3300	460		7.1	3.2×10^{-11}
	Temperature (℃)	-6.4	1.9	-0.22	-3.4	8.0×10^{-4}
	Pressure (Pa)	-3.1	0.50	-0.42	-6.2	3.4×10^{-9}
5	(Constant)	3600	470		7.7	9.7×10^{-13}
	Pressure (Pa)	-3.6	0.49	-0.48	-7.3	1.1×10^{-11}

$$Z'_Y = \beta_1 Z_{X1} + \beta_2 Z_{X2} + \ldots\ldots + \beta_n Z_{Xn} \quad (3)$$

where β' s and Z' s are the standardised coefficient and Z-scores, respectively.

Using the backward regression analysis, barometric pressure was found to be the most significant influencing meteorological parameters on ^{222}Rn data with an R-square value of 22% (Table 2). On the other hand, it must be noted that soil gas radon fluctuation does not only depend on meteorological factors but also on geophysical phenomena like seismic activity. Of the three significant variables, temperature and pressure have a reverse correlation with ^{222}Rn flux while humidity has a positive one. In other words, temperature and pressures suppressed ^{222}Rn counts while humidity enhanced it. Due to atmospheric pumping effect poor air radon was forced

into the upper layer of the soil during rose in pressure hence diluting the radon concentration[32, 42-46]. While the reverse correlation of temperature with ^{222}Rn might be explained as the masking effect of temperature by pressure as the two parameters were observed to have a significant positive correlation (r=0.3, p=0.0001) (Table 1). It has been reported[44-48] that raised in air temperature caused soil-air radon to expanded and hence enhanced radon exhalation. Hence the observed reversed correlation leads us to nothing but the effect of air temperature was masked by pressure which has been observed in the previous study[32]. Now the independent predictors have been narrowed down to humidity and pressure. It has been also reported that presence of humidity up to 15-17% by weight (optimum level)[49] in the soil enhanced ^{222}Rn emanation by absorbing its recoil energy which prevent it from burying in the adjacent soil grain[50]. Pressure being the most influential variable, it was unlikely to observe significant radon anomaly due to humidity hence we are left out with one potential candidate, that is, geophysical processes discuss in the following section. In general, it must also be noted that though a significant correlation was observed between radon and some meteorological data, the correlation coefficients were mostly weak except for pressure. All the above observation points toward geophysical phenomena especially seismic activity as the culprit behind radon anomaly but not meteorological factors in cent per cent.

4.2. Estimation of ^{238}U and ^{232}Th from ^{222}Rn and ^{220}Rn respectively

The radon and thoron counts were converted into their respective concentrations using equation (4)[1]

$$C_{Rn} = \frac{C}{3EVe^{\lambda t}} \tag{4}$$

Where C is the net count rate (count per second, s^{-1}) of ^{222}Rn or ^{220}Rn, E is the efficiency of counting, V is volume of the sampler (m^3), λ is the decay constant of ^{222}Rn or ^{220}Rn, t is the time delay post-sampling (s) and 3 represent the three alphas in the respective decay chain of ^{222}Rn and ^{220}Rn.

For obtaining ^{222}Rn flux the monitor was operated in closed loop manner (Fig. 3a) in radon mode with 15 minutes cycle for 3 hours at each of the sampling spots. Least fitting of the built up radon concentration with elapse time was perform for each spot. Then average value of the built up rate $C(t)$, of the 9 spot was taken and substitute to assessed ^{222}Rn flux using equation (5)[1].

$$C(t) = C_0 + k\frac{A}{V}ft \tag{5}$$

Where C_0 is the initial concentration (Bq m^{-3}), k is the factor by which the initial flux drops while the gas inside the accumulator pass through state of uniform mixing prior to deployment to state of diffusive mixing post to deployment, A is the surface area of the opening of the accumulator (m^2), V is the effective volume of the sampling device (m^3), f is the flux of radon (Bq m^{-2} s^{-1}) and t is the measurement time (s).

On the other hand the ^{220}Rn flux was obtained using equation (6)[1]

$$f = \frac{C_{eq}V\lambda}{A} \tag{6}$$

Where C_{eq} is the ^{220}Rn equilibrium concentration (Bq m^{-3}), V is the effective volume of the sampling device (m^3), λ is the thoron decay constant and A is the surface opening area of the accumulator (m^2).

To obtain the equilibrium ^{220}Rn concentration, the monitor was operated in ^{220}Rn mode with 15 minutes cycle for 1 hour in each of the sampling spot. Then average of the last three concentration value from the 9 spots was taken which represent the C_{eq}[1]. The first reading was neglected as it could be corrupted by external factors.

Now to obtain ^{226}Ra content of the soil which is in equilibrium with ^{238}U[1], the mass exhalation rate of the sampling region was obtained. For this soil sample from the 9 sampling spots were taken to the laboratory and put them in a mass exhalation chamber of volume 5×10^{-4} m^3 (Fig. 3c). The detector probe of the monitor was directly mounted on the mass exhalation chamber using the provided slight tight mechanism preventing leakage of sample gas. The monitor was operated in ^{222}Rn mode with 60 minutes cycle for 12 hours. In this mode only alpha particle of radon was counted, as thoron was protected from entering the scintillation cell by the thoron discriminator, placed at the entrance of the cell. The build up radon concentration with elapse time was least fitted to obtained the build up rate $C(t)$ and substituted in equation (7)[1] to obtained the mass exhalation rate.

$$C(t) = \left(\frac{J_m M}{V}\right)t + C_0 \tag{7}$$

Where J_m is the mass exhalation rate (Bq kg^{-1} s^{-1}), M is mass of the sample (kg), V is the effective volume of the detector (m^3), t the measurement time and C_0 the ^{222}Rn concentration at time $t = 0$.

Using the value of J_m from equation (7), the ^{226}Ra content which is equilibrium concentration with ^{238}U may be estimated using equation (8)[1, 2]

Table 3. Details of ^{222}Rn, ^{220}Rn, ^{238}U and ^{232}Th data's obtained from the study area

	^{222}Rn	^{220}Rn	Ratio (^{220}Rn/^{222}Rn)
Bq m^{-3}	8143.2	13822.9	1.7
Bq m^{-2} s^{-1}	0.015	2.7	180
	^{238}U	^{232}Th	Ratio (^{232}Th/^{238}U)
Bq kg^{-1}	16.9	49.7	2.9

$$J_m = RE\lambda \quad (8)$$

Where R is ^{226}Rn content of the soil in Bq kg^{-1}, E is the emanation coefficient of ^{222}Rn (0.1-0.3 in soil)[1], λ is the radioactive decay constant of ^{222}Rn.

The ^{232}Th equivalent concentration of ^{224}Ra content was obtained using the flux obtained in equation (6)[1, 2] as follow

$$f = \lambda LR\rho E \quad (9)$$

Where f is the ^{220}Rn flux at the soil-air interface, λ is the ^{220}Rn decay constant, L is the diffusion length of ^{220}Rn in soil (0.013 m)[1], R is the ^{224}Ra content in the soil, ρ is the density of the soil matrix and E is the emanation coefficient of ^{220}Rn (0.14)[1].

From equation (4) the average ^{222}Rn and ^{220}Rn concentration of the study area was found to be 8143.2 Bq m^{-3} and 13822.9 Bq m^{-3}, respectively. From equation (5) and (6) the flux of ^{222}Rn and ^{220}Rn at the soil-air interface within the grid was found to be 0.015 Bq m^{-2} s^{-1} and 2.7 Bq m^{-2} s^{-1}, respectively. Again from equation (7) the mass exhalation rate of the region was found to be 0.030 Bq kg^{-1} h^{-1}. Substituting this value and the other conventional parameters given in IAEA[1] in equation (8) the ^{226}Ra content of the soil was found to be 16.9 Bq kg^{-1}. On the other hand, from equation (9) the ^{224}Ra content of the study area was found to be 49.7 Bq kg^{-1}. Since the concentration of ^{226}Ra and ^{224}Ra were in equilibrium with their respective parent nuclei ^{238}U and ^{232}Th in soil[1]. Hence the concentration of ^{238}U and ^{232}Th in soil of the study area may be expressed as 16.9 Bq kg^{-1} and 49.7 Bq kg^{-1}, respectively. The ^{220}Rn to ^{222}Rn concentration, ^{220}Rn flux to ^{222}Rn flux and ^{232}Th to ^{238}U content has a ratio of 1.7, 180 and 2.9, respectively (Table 3). The observation clearly depicts that the higher ^{232}Th content of the region reflects in higher concentrations and flux of its daughter nuclei (^{220}Rn) to that of its isotope (^{222}Rn) of ^{238}U decay chain. When compared to that of the worldwide average, concentrations of the isotope pair falls within the given range (10^3-10^5 Bq m^{-3} in soil) given by IAEA[1]. The obtained ^{222}Rn flux was in close agreement with the worldwide average (15-20 mBq m^{-2} s^{-1}) given by UNSCEAR[51] while ^{220}Rn flux surpass the reported range (1-1.9 Bq m^{-2} s^{-1})[51]. Also the obtained activity concentration of ^{238}U and ^{232}Th were found to be respectively lower and higher than their corresponding worldwide average of 35 Bq kg^{-1} and 30 Bq kg^{-1} given in UNSCEAR[34]. At the same time both the activity concentration of ^{238}U and ^{232}Th were much lower than the critical value of 1000 Bq kg^{-1} set by IAEA[35]. Hence in terms of health hazard no radiological risk was observed at the study area.

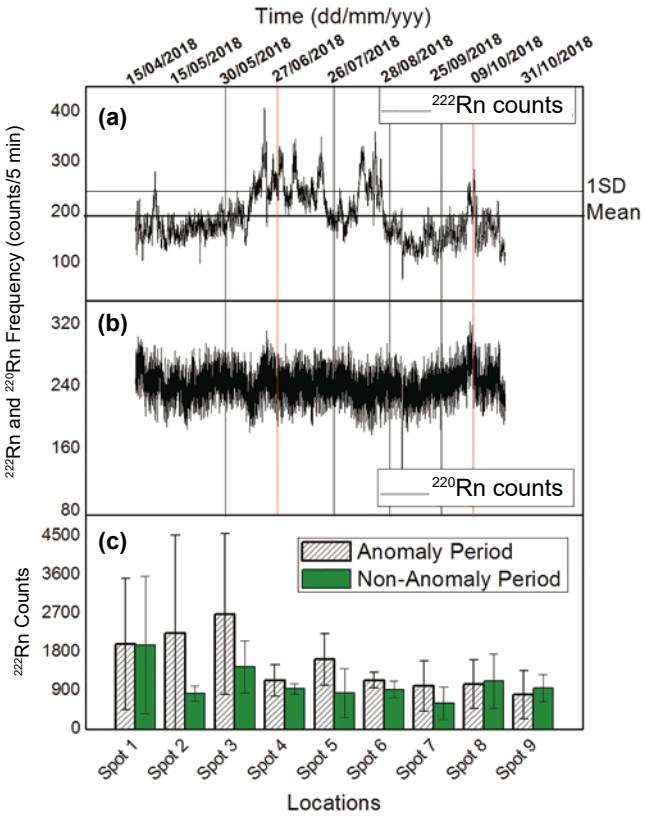

Fig. 5. Plot of (a) 15 minutes cycle ^{222}Rn data of the CMS classifying *in-situ* ^{222}Rn data of Mat fault into anomaly period and non-anomaly period data generated between April 15, 2018 and October 31, 2018. The dates of experiment were represented by vertical red and black lines, indicating anomaly period and non-anomaly period data's, respectively, (b) 15 minutes cycle ^{220}Rn data at the soil-air interface of the CMS between April 15, 2018 and October 31, 2018, (c) Average of anomaly period and non-anomaly period ^{222}Rn counts data for each of the nine spots from the rectangular grid at Mat fault between May, 2018 and October, 2018.

4.3. Comparative analysis of soil-air interface in-situ radon data with Continuous Data

Measurement of ^{222}Rn and ^{220}Rn counts data at Mat fault was carried out on the following dates: May 30, 2018; June 27, 2018; July 26, 2018; August 28, 2018; September 25, 2018 and October 9, 2018. To differentiate them into anomaly and non-anomaly period data, the negligibly

meteorological influence data of the CMS was adopted. The nature of radon data of the CMS has been discussed in section 3.2 and 4.1. There was no definite criterion for assigning radon anomalies; hence every author defines it appropriate to its own data[11]. For example, anomalies of atmospheric radon data 5 m above the ground surface at Kobe Pharmaceutical University was observed at 3σ (σ = standard deviation) from the mean[18-21]. On the other hand, several authors[16, 27, 28, 30, 31, 52-55] monitoring soil radon data adopt the mean plus 'n' times standard deviation (SD) criterion (n = 1, 2, 3,.....). All of them including authors[16, 27, 28, 30, 31] who had monitors at the present study area by passive sampling reports radon anomalies at 2σ, 1.5σ as well as at 1σ prior to earthquakes. Recently, Sahoo and group[56] reports fluctuation in the Instantaneous Energy of time series radon data above 2σ and 1σ before some local earthquakes at Kutch, Gujarat, India. All these reports, specifically of radon data at soil signify that accumulated strain at local distance from the monitoring station resulted in increase of radon concentration above 1σ from its mean or more. The mean plus 'n' times standard deviation criterion was as well adopted by the authors and raise in radon data above 1σ(1SD) was considered as radon anomaly (Fig. 5a). The reason behind assigning radon anomaly at 1σ is to completely identify radon data with the slightest geophysical characteristic nature from the normal one based on the fact that anomalies above 1σ were associated with earthquakes[16, 27, 28, 30, 31, 52-55]. Besides, the meteorological influence on the radon data was highly minimised as discussed in section 3.2 and 4.1 above. Hence, any fluctuation above 1σ was confidently taken as radon anomaly due to local geophysical phenomena. Such that, if radon data were generated at Mat fault by the time radon data at the CMS cross 1σ, they were taken as anomaly period data otherwise a non-anomaly period data. By this criterion radon data of May 30, 2018; July 26, 2018; August 28, 2018 and September 25, 2018 were considered anomaly period data while those of June 27, 2018 and October 9, 2018 were taken as non-anomaly period data. In Fig. 5a the 1σ line was represented by a horizontal line and dates of the experiment by a vertical line. The vertical red and black lines represent anomaly and non-anomaly data, respectively. Thoron data of the CMS within the said period was also given in Fig. 5b. Now radon counts during the anomaly and non-anomaly period from each sampling spots were compared. It has been observed that in 78% of the spots (7 out of 9 spots), the radon counts were higher during anomaly period (Fig. 5c). The observation reveals that majority of the sampling spot were able to show higher radon exhalation during geophysical activity which in turn indicates the fault was active[16, 26-33]. The observation was in agreement with the experimentally demonstrated analytical model of Sahoo and Gaware[2]. In their model they suggested that the radon concentration at the sub-soil was low as compare to that of deep soil. Hence perturbation of the radon concentration was more pronounce and easier to detect than that of deep soil during stress release. Hence it may be concluded during the study period the radon data response well to geophysical processes.

5. Conclusion

The study shows presence of meteorological effect on ^{222}Rn and ^{220}Rn data's at the ground surface. Relative humidity and barometric pressure were found to be the enhancing and suppressing factors of ^{222}Rn count, respectively while pressure was found to be the most influencing factors. The observed correlations were mostly weak except for pressure where it was found to be moderate. Hence radon anomaly under such condition was assumed as a result of geophysical activity. No strong correlation was observed between ^{220}Rn data and meteorological factors, also the correlations were insignificant except for rainfall. The weak correlation between the isotope pair and most of the meteorological factors shows the effectiveness of the shading provided in the monitoring station. It also signifies the possibility of reducing the meteorological effect physically to a substantial amount. Results of the study also shows that the obtained ^{222}Rn (concentration and flux) and ^{238}U data were in agreement and lower than their corresponding worldwide average, respectively. The ^{220}Rn concentration also agrees well with the worldwide average, while its flux and parent nuclei (^{232}Th) content surpasses it. The higher ^{232}Th content reflects the higher concentration and flux of ^{220}Rn data to that of its isotope. Based on the critical value set by IAEA[35], no radiological hazard was found from ^{238}U and ^{232}Th of the study area. Upon comparing the *in-situ* data at Mat fault with continuous data of the CMS, it was observed that both the location response well to geophysical activity of the region. This signifies the reason behind the unison variation of radon data 57 km apart from each other could be nothing but geophysical phenomena. Considering the limited studies and literature on radon monitoring, the authors hopes the present data (continuously generated till date) will serve as a vital role in future seismic precursory study. Direct correlation of the data with seismic data of the region was neglected as the authors find the data was only for a period of six months and immature for such prediction studies. Since this study suggest that radon anomaly of the region were due to geophysical phenomena especially seismic activity, upon accumulating a substantial amount of data its correlation with seismic activity will be followed up shortly.

Acknowledgements

This work was supported financially by DAE-BRNS, BARC, Mumbai, India [Sanction Order No.:36(4)/14/66/2014-BRNS/36024 Dt.26.02.2016.]

Funding

This study was funded by DAE-BRNS, BARC, Mumbai, India (No.:36(4)/14/66/2014-BRNS/36024 Dt.26.02.2016.).

Conflict of Interest

The authors declare that they have no conflict of interest.

References

1. IAEA. Measurement and Calculation of Radon Releases from NORM Residues. Vienna: International Atomic Energy Agency; 2013. TRS 474: p.1–74.
2. Sahoo BK, Gaware JJ. Radon in ground water and soil as a potential tracer for uranium exploration and earthquake precursory studies. SRESA's International Journal of Life Cycle Reliability and Safety Engineering. 2016;5(3):21–9.
3. Sahoo BK, Mayya YS. Two dimensional diffusion theory of trace gas emission into soil chambers for flux measurements. Agr Forest Meteorol. 2010;150(9):1211–24.
4. Dubinchuk VT. Radon as a precursor of earthquakes. Isotopic and geochemical precursors of earthquakes and volcanic eruptions. Vienna: International Atomic Energy Agency; 1993. TECDOC-726: p.9–22.
5. Yasuoka Y, Shinogi M. Anomaly in atmospheric radon concentration: a possible precursor of the 1995 Kobe, Japan, earthquake. Health Phys. 1997;72(5):759–61.
6. King CY. Radon emanation on San Andreas fault. Nature. 1978;271(5645):516–9.
7. King CY, King BS, Evans WC, Zhang W. Spatial radon anomalies on active faults in California. Appl Geochemistry. 1996;11(4):497–510.
8. Shapiro MH, Melvin JD, Tombrello TA, Mendenhall MH, Larson PB, Whitcomb JH. Relationship of the 1979 Southern California radon anomaly to a possible regional strain event. J Geophys Res: Solid Earth. 1981;86(B3):1725–30.
9. Singh M, Ramola RC, Singh B, Singh S, Virk HS. Subsurface soil gas radon changes associated with earthquakes. Int J Radiat Appl Instrum D. 1991;19(1-4):417–20.
10. Ghosh D, Deb A, Haldar S, Sahoo SR, Sengupta R. Radon Time Series and Earthquake Signals-a Study by SSNTD at Matigara (Darjeeling), India. Earth Science India. 2009;2(II):76–82.
11. Igarashi G, Wakita H. Groundwater radon anomalies associated with earthquakes. Tectonophysics. 1990;180(2-4):237–54.
12. Virk HS, Singh B. Radon anomalies in soil-gas and groundwater as earthquake precursor phenomena. Tectonophysics. 1993;227(1-4):215–24.
13. Wakita H. Geochemical challenge to earthquake prediction. Proceedings of the National Academy of Sciences. 1996;93(9):3781–6.
14. Zmazek B, Živčić M, Vaupotič J, Bidovec M, Poljak M, Kobal I. Soil radon monitoring in the Krško Basin, Slovenia. Appl Radiat Isot. 2002;56(4):649–57.
15. Walia V, Lin SJ, Hong WL, Fu CC, Yang TF, Wen KL, *et al.* Continuous temporal soil-gas composition variations for earthquake precursory studies along Hsincheng and Hsinhua faults in Taiwan. Radiat Meas. 2009;44(9-10):934-9.
16. Singh S, Jaishi HP, Tiwari RP, Tiwari RC. Time series analysis of soil radon data using multiple linear regression and artificial neural network in seismic precursory studies. Pure Appl Geophys. 2017;174(7):2793–802.
17. Chowdhury S, Deb A, Nurujjaman M, Barman C. Identification of pre-seismic anomalies of soil radon-222 signal using Hilbert–Huang transform. Nat Hazards. 2017;87(3):1587–606.
18. Iwata D, Nagahama H, Muto J, Yasuoka Y. Non-parametric detection of atmospheric radon concentration anomalies related to earthquakes. Sci Rep. 2018;8(1):1–9.
19. Kawada Y, Nagahama H, Omori Y, Yasuoka Y, Ishikawa T, Tokonami S, *et al.* Time-scale invariant changes in atmospheric radon concentration and crustal strain prior to a large earthquake. Nonlin Processes Geophys. 2007;14:123–30.
20. Omori Y, Yasuoka Y, Nagahama H, Kawada Y, Ishikawa T, Tokonami S, *et al.* Anomalous radon emanation linked to preseismic electromagnetic phenomena. Nat Hazards Earth Syst Sci. 2007;7:629–35.
21. Yasuoka Y, Kawada Y, Nagahama H, Omori Y, Ishikawa T, Tokonami S, *et al.* Preseismic changes in atmospheric radon concentration and crustal strain. Phys Chem Earth ABC. 2009;34(6-7):431–4.
22. Yasuoka Y, Kawada Y, Omori Y, Nagahama H, Ishikawa T, Tokonami S, *et al.* Anomalous change in atmospheric radon concentration sourced from broad crustal deformation: A case study of the 1995 Kobe earthquake. Appl Geochemi. 2012;27(4):825–30.
23. Chaudhuri H, Bari W, Iqbal N, Bhandari RK, Ghose D, Sen P, *et al.* Long range gas-geochemical anomalies of a remote earthquake recorded simultaneously at distant monitoring stations in India. Geochem J. 2011;45(2):137–56.
24. Chaudhuri H, Ghose D, Bhandari RK, Sen P, Sinha B. A geochemical approach to earthquake reconnaissance at the Baratang mud volcano, Andaman and Nicobar Islands. J Asian Earth Sci. 2012;46:52–60.
25. BIS. Indian Standard criteria for earthquake resistant design of structure part1-general provisions and buildings. BIS IS 1893 (Part 1) New Delhi; 2002.
26. Jaishi HP, Singh S, Tiwari RP, Tiwari RC. Radon and thoron anomalies along Mat fault in Mizoram, India. J Earth Syst Sci. 2013;122(6):1507–13.
27. Jaishi HP, Singh S, Tiwari RP, Tiwari RC. Temporal variation of soil radon and thoron concentrations in Mizoram (India), associated with earthquakes. Nat hazards. 2014;72(2):443–54.
28. Jaishi HP, Singh S, Tiwari RP, Tiwari RC. Correlation of radon anomalies with seismic events along Mat fault in Serchhip District, Mizoram, India. Appl Radiat Isot. 2014a;86:79–84.
29. Jaishi HP, Singh S, Tiwari RP, Tiwari RC. Analysis of soil radon data in earthquake precursory studies. Ann Geophys. 2014b;57(5):0544.
30. Singh S, Jaishi HP, Tiwari RP, Tiwari RC. Variations of soil radon concentrations along Chite Fault in Aizawl district, Mizoram, India. Radiat Prot Dosim. 2014;162(1-2):73–7.
31. Singh S, Jaishi HP, Tiwari RP, Tiwari RC. A study of variation in soil gas concentration associated with earthquakes near Indo-Burma Subduction zone. Geoenvironmental Disasters. 2016;3(1):22.
32. Thuamthansanga T, Sahoo BK, Tiwari RC, Sapra BK. A study on the anomalous behaviour of Radon in different depths of soil at a tectonic fault and its comparison with time-series data at a distant

continuous monitoring station. SN Applied Sciences. 2019;1(7):683.

33. Thuamthansanga T, Tiwari RC, Tiwari RP, Sahoo BK. Correlation Study of ^{222}Rn Production Rate and Exhalation Rate with Geophysical Process at Mat Fault in Mizoram. Journal of International Academy of Physical Sciences. 2020b;24(1):83–93.
34. UNSCEAR. Sources and effects of ionizing radiation. Annex B: Exposures from natural radiation sources. United Nations; 2000.
35. IAEA. Safety Standards Series No. RS-G-1.7: Application of the concepts of exclusion, exemption and clearance. Safety Guide. Vienna: International Atomic Energy Agency; 2004.
36. Nandy DR. Geodynamics of Northeastern India and the adjoining region. Calcutta: ABC Publications; 2001. p.209.
37. Malsawma J, Lalnuntluanga P, Badekar A, Sangode SJ, Tiwari RP. Magnetic polarity stratigraphy of the Bhuban succession, Surma Group, Tripura-Mizoram accretionary belt. J Geol Soc India. 2010;76(2):119–33.
38. Tiwari RP. Status of seismicity in the northeast India and earthquake disaster mitigation. ENVIS Bull. 2002;10(1):15–25.
39. Gaware JJ, Sahoo BK, Sapra BK,Mayya YS. Indigenous development of online radon and thoron monitors for applications in Uranium mining and Thorium processing facilities. Founder' s Day Special Issue, BARC Newsletter: DAE EA. 2011;30:149-153 [cited 2020 June 29]. Available from:http://www.barc.gov.in/publications/nl/2011/fday2011.html.
40. Thuamthansanga T, Tiwari RC, Sahoo BK, Datta D. Analysis of Meteorological Influence on Exhalation of ^{222}Rn and ^{220}Rn Gases at Mat Fault. In: Tiwari RC editor. Radon: Detection, Exposure and Control., USA: Nova Science Publishers, Inc; 2020. Chapter 17 [cited on 2020 June 29]. Available from: https://novapublishers.com/shop/radon-detection-exposure-and-control/
41. Thuamthansanga T, Sahoo BK, Tiwari RC. Study of the Influencing nature of meteorological factors Air temperature and Relative Humidity on the exhalation process of ^{222}Rn/^{220}Rn gases at Mat fault. J Appl Fundam Sci. 2020a;6(1):41.
42. Gingrich JE. Radon as a geochemical exploration tool. J Geochem Explor. 1984;21(1-3):19–39.
43. Klusman RW and Webster JD. Preliminary analysis of meteorological and seasonal influences on crustal gas emission relevant to earthquake prediction. B Seismol Soc Am. 1981;71(1):211–22.
44. Ramola RC, Singh M, Sandhu AS, Singh S and Virk HS. The use of radon as an earthquake precursor. Int J Radiat Appl Instrum E. 1990;4(2):275–87.
45. Segovia N, Seidel J, Monnin M. Variations of radon in soils induced by external factors. J Radioanal Nucl Chem. 1987;119(3):199–209.
46. Singh MW, Ramola RC, Singh S, Virk HS. The influence of meteorological parameters on soil gas Radon. J Assoc Expl Geophys. 1988;IX(2):85–90.
47. Virk HS, Walia V, Sharma AK, Kumar N, Kumar R. Correlation of radon anomalies with microseismic events in Kangra and Chamba valleys of NW Himalaya. Geofís Int. 2000;39(3):221–7.
48. Walia V, Virk HS, Yang TF, Mahajan S, Walia M, Bajwa BS. Earthquake prediction studies using radon as a precursor in NW Himalayas, India: a case study. TAO: Terr Atmos Ocean Sci. 2005;16(4):775.
49. Stranden E, Kolstad AK, Lind B. The influence of moisture and temperature on radon exhalation. Radiat Prot Dosim. 1984;7(1-4):55–8.
50. Asher-Bolinder S, Owen DE, Schumann RR. A preliminary evaluation of environmental factors influencing day-to-day and seasonal soil–gas radon concentrations. In: Field Studies of Radon in Rocks, Soils and Waters. USGS Bulletin. 1971:23–31.
51. UNSCAER. Ionizing Radiation: Sources and Biological Effects. Annex D: Exposures to Radon and Thoron and their decay products. United Nations; 1982.
52. Deb A, Gazi M, Ghosh J, Chowdhury S, Barman C. Monitoring of soil radon by SSNTD in Eastern India in search of possible earthquake precursor. J Environ Radioact. 2018;184:63–70.
53. Ghosh D, Deb A, Sengupta R, Patra KK, Bera S. Pronounced soil-radon anomaly-Precursor of recent earthquakes in India. Radiat Meas. 2007;42(3):466–71.
54. Ramola RC, Prasad Y, Prasad G, Kumar S, Choubey VM. Soil-gas radon as seismotectonic indicator in Garhwal Himalaya. Appl Radiat Isot. 2008;66(10):1523–30.
55. Vaupotič J, Riggio A, Santulin M, Zmazek B, Kobal I. A radon anomaly in soil gas at Cazzaso, NE Italy, as a precursor of an ML= 5.1 earthquake. Nukleonika. 2010;55:507–11.
56. Sahoo SK, Katlamudi M, Barman C, Lakshmi GU. Identification of earthquake precursors in soil radon-222 data of Kutch, Gujarat, India using empirical mode decomposition based Hilbert Huang Transform. J Environ Radioact. 2020;222:106353.